



3D Rigid registration by cylindrical phase correlation method

Jakub Bican^{a,b,*}, Jan Flusser^a

^a Institute of Information Theory and Automation, Pod vodárenskou věží 4, 18208 Prague 8, Czech Republic

^b Faculty of Mathematics and Physics, Charles University in Prague, Ke Karlovu 3, 121 16 Prague 2, Czech Republic

ARTICLE INFO

Article history:

Received 9 January 2008

Received in revised form 12 March 2009

Available online 2 April 2009

Communicated by G. Borgefors

Keywords:

Image registration
Phase correlation
Cylindrical transform
Rigid body transform

ABSTRACT

Spatial alignment is an essential step before any further processing (such as fusion and change detection) of multiframe images can be done. We present a new algorithm that aligns translated and rotated pair of 3D images by means of phase correlation method (PCM). PCM is a computationally efficient method for translation estimation. We generalize a known polar-mapping approach of 2D image registration by PCM to estimate mutual rotation of a pair of 3D images about known axis. An improvement of this technique is given to eliminate influence of noise and image differences in non-ideal conditions. Finally, an iterative optimization procedure called cylindrical phase correlation method (CPCM) is proposed which uses these techniques in rigid body registration tasks. We utilize CPCM to register 3D tomographic images of human brain and study its performance in several experiments. CPCM shows extreme robustness to noise and is able to reliably and rapidly align even highly misregistered images.

© 2009 Elsevier B.V. All rights reserved.

1. Introduction

Image registration plays a major role in multiframe image processing. The purpose of image registration is to geometrically align two or more images differing by the imaging time, viewpoint, sensor modality and/or the subject of the images. Among many areas where the image registration is employed (such as remote sensing and computer vision), medical image processing is one of the most important.

Image registration methods are usually classified into two main groups (e.g. Zitová and Flusser, 2003). Feature-based methods incorporate a feature selection step to detect a set of control points, a feature matching step to find the correspondences between two sets of control points and a transform model estimation step to determine parameters of the selected transformation from the correspondences. Very popular in medical image registration – especially in tomographic brain image registration – is an optimization scheme that aims to find, by a certain numerical optimization process, an extreme of similarity or dissimilarity measure on a multidimensional space of parameters of a selected transform model. Methods based on mutual information are state-of-the-art among these approaches (e.g. Gholipour et al., 2007).

Fourier methods form a special group of approaches based on the phase correlation method (PCM). PCM was first introduced

by Kuglin and Hines (1975) as a fast and robust method for estimation of inter-image shifts. The method was extended by De Castro and Morandi (1987) to register translated and rotated images and later by Reddy and Chatterji (1996) to register translated, rotated and scaled images. The authors use a log-polar transform of shift invariant spectral magnitudes to turn rotation and scaling to translation handled analogically by PCM. This approach is not applicable for 3D image registration as there is no mapping that converts rotation to translation in 3D.

Keller et al. (2006) introduced an algorithm for registration of rotated and translated 3D volumes based on the pseudopolar Fourier transform. Their approach uses the pseudopolar representation of spectral magnitudes to find the rotation axis and to estimate the rotation angle without using interpolation.

Other authors aim to refine the precision of PCM to subpixel level. Foroosh et al. (2002) estimate the subpixel shifts by analyzing polyphase decomposition of cross-power spectrum. Stone et al. (2001) first eliminate the effect of aliasing and then use least-squares fit to 2D phase difference data. As this is a difficult task, authors of Hoge (2003) and Hoge and Westin (2005) separate the shift estimation in every dimension by SVD or high-order SVD of cross-power spectrum. An improvement of robustness of this approach is given in (Keller et al., 2004).

All the Fourier approaches mentioned above estimate the rotations on the shift invariant spectral magnitudes of the images. In cases of images with a low structural nature of spectral magnitudes (e.g. many medical imaging modalities) we find this difficult and unreliable as most of the information important for the PCM (e.g. image edges) has been lost as the image phase was discarded from the rotation estimation. Landmark and metric optimization

* Corresponding author. Address: Institute of Information Theory and Automation, Pod vodárenskou věží 4, 18208 Prague 8, Czech Republic. Tel.: +420 266052586; fax: +420 284680730.

E-mail addresses: jakub.bican@matfyz.cz (J. Bican), flusser@utia.cas.cz (J. Flusser).

methods can be used even for registration of higher-order transforms (elastic registrations) and for multi-modal registrations, but for landmark methods there is a serious problem in robust detection and matching significant landmarks in certain modalities and metric optimization methods face trade-offs between convergence speed and reliability. Both approaches are usually sensitive to noise and their performance and reliability decrease with increasing misregistration of the data.

In this paper, we present a new way of employing PCM to register 3D images to use its speed and robustness in 3D rigid registration tasks. Our method is based on cylindrical coordinate mapping of the image in spatial domain and iteratively uses PCM to estimate the update of rigid body transform with respect to certain transform components: rotation or translation. We experimentally study the method's performance in the case of tomographic brain image registration tasks.

2. Phase correlation method

Phase correlation method by Kuglin and Hines (1975) takes advantage of *Fourier shift theorem* that relates the phase information of spectrums of a reference image f_M and its shifted copy. If moving image f_M is the shifted copy of f_M then the spectra of the images are according to the Fourier shift theorem related as follows:

$$F_M(\vec{\omega}) = e^{i(\omega_x \Delta x + \omega_y \Delta y + \omega_z \Delta z)} F_R(\vec{\omega}),$$

$$\mathfrak{F}^{-1}\left(\frac{F_M(\vec{\omega})}{F_R(\vec{\omega})}\right) = \mathfrak{F}^{-1}\left(e^{i(\omega_x \Delta x + \omega_y \Delta y + \omega_z \Delta z)}\right) = \delta(\vec{x} + \Delta\vec{x}).$$

Quotient of spectrums F_M and F_R is in practise (even if f_M is not exactly the shifted copy of f_R) computed as

$$\text{corr}(\vec{\omega}) = \mathfrak{F}^{-1}\left(\frac{F_M F_R^*}{|F_M| |F_R|}\right),$$

so that PCM computes the correlation of whitened images (images with $|F| = 1$).

Thus, locating a peak in a correlation surface corr results in offset $\Delta\vec{x}$ that can be used to align f_R and f_M at pixel-level

$$PCM(f_R, f_M) = \Delta\vec{x} = \text{argmax}_{\vec{x}}(\text{corr}(\vec{x})).$$

3. Cylindrical phase correlation method

In this section, we introduce new image registration algorithms. First, we describe a technique for using PCM to find a rotation angle in case two volumes are only rotated about a known axis. Then, we give important improvements that increase the performance of the technique in non-ideal conditions. Finally, we use this technique in an iterative algorithm that registers volumes differing by a rigid body transform.

3.1. Finding rotation with known axis

Now consider two 3D images f_R and f_M that are related by a rotation.

In the 2D case, it is possible to convert the rotation around some central point to a translation by polar transforming the images with the origin of the polar coordinates located in the centre of the rotation. The angle of rotation then can be determined by using 2D version of PCM described above. The direct generalization of this approach for the 3D case by using spherical coordinates does not work as these coordinates do not convert 3D rotation to a translation. If the rotation axis is known, PCM can be used on cylindrically mapped images to estimate the rotation angle.

Let us represent the rotation by axis \vec{v} and angle α and assume the rotation axis \vec{v} is known. For simplicity let us suppose, that the rotation axis is the z-axis of the Cartesian coordinate system. Transformation to cylindrical coordinates about z-axis is computed as $f^*(\alpha, r, z) = f(r \cos \alpha, r \sin \alpha, z)$. Rotation of the image f_R by an angle $\Delta\alpha$ has the same effect as shifting the periodically extended image f^* by $\Delta\vec{x}^* = (\Delta\alpha, 0, 0)$

$$f_M(\vec{x}) = f_R(R_z(\Delta\alpha)\vec{x}),$$

$$f_M^*(\vec{x}^*) = f_R^*\left((\vec{x}^* + \Delta\vec{x}^*) \bmod S_{f_R}^*\right),$$

where $R_z(\Delta\alpha)$ is the rotation matrix for rotation about z-axis (Baker, 1998–2007) and $S_{f_R}^*$ is the size of the image f_R^* . (Asterisk superscript (*) denotes a cylindrical coordinate system.)

Now, it is clear that the rotation angle $\Delta\alpha$ can be estimated by PCM on cylindrically transformed images f_R^* and f_M^* .

In fact, this technique of rotation estimation is very similar to that of Reddy and Chatterji (1996). In every plane orthogonal to the axis of the cylinder, the image is transformed to polar coordinates that convert rotation about the axis to translation. PCM of all transformed planes then computes overall rotation around the axis. The cylindrically (or polar) transformed image is periodic in the angular direction (after passing angle 2π we may continue again from 0). As well, Fourier transform of the discrete and bounded image assumes that the image is periodically extended beyond its bounds. Therefore the intrinsic presumption of periodicity is fulfilled in case of PCM on cylindrically mapped images.

3.2. Improving the performance

The approach described in the previous section has two main drawbacks. The first one is caused by performing computations in discrete domain: when making cylindrical transform of the images, it is necessary to use higher-order interpolation, because the cylindrical transform (alike the polar transform) is sampling the space very non-uniformly.

The second drawback is that the voxels of the original volume located near the axis of the cylinder have much greater impact than the voxels located at the perimeter. If the angular and radial coordinates are sampled so that the perimeter of the cylinder is not subsampled and no information is lost, every voxel near the axis is stretched (or interpolated) to several voxels, while the voxels at the perimeter are resampled approximately one-to-one. Moreover, the PCM gives the same significance to well-sampled voxels at the perimeter as to resampled voxels originating from the voxels near the axis, which are also highly affected by an interpolation error.

These drawbacks led us to develop technique computing PCM separately for every *layer* of the cylinder defined by a fixed radius. Every such layer has a different angular resolution that suitably samples the original data: layer at radius r is in angular direction sampled by $2\pi r$ samples, i.e. with resolution (spacing) $2\pi/2\pi r = 1/r$ radians.

$$I_R^r(\alpha, z) = f_R^*(\alpha, r, z) \quad \forall \alpha = 0, 1/r, \dots, (2\pi - 1/r),$$

$$\forall z = 0, 1, \dots, S_{f_R}^z. \tag{1}$$

Corresponding layers from reference and moving image are registered by PCM which results in a correlation surface that provides a degree of match for each angle. Correlation surfaces from all layers are then summed up to obtain the global correlation surface

$$\text{corr}_{\text{imp}}(\alpha, z) = \sum_{r=1}^{S_{f_R}^r} \mathfrak{F}^{-1}\left(\frac{\mathbf{L}_R \mathbf{L}_M^*}{|\mathbf{L}_R| |\mathbf{L}_M|}\right)(\alpha, z), \tag{2}$$

where $\mathbf{L}_{R|M}$ are Fourier transforms of layers $l_{R|M}$. Off-grid image values in Eq. (1) are computed using linear interpolation. Off-grid layer correlation surface values in Eq. (2) are computed using nearest-neighbour interpolation. Finally, position of the highest peak in the combined correlation surface corr_{imp} provides the final result of the registration

$$\text{IRE}(f_R, f_M) = \text{argmax}_{\alpha, z} (\text{corr}_{\text{imp}}(\alpha, z)).$$

Properties of the cylinder – i.e. number of layers $S_{f_R}^r$, inter-layer spacing, and height of the cylinder $S_{f_R}^z$ – are determined with the strategy to rather oversample than subsample. The number of layers is determined using the largest size and lowest spacing across all dimensions of both reference and moving image. The height of the cylinder is the double of the number of layers with the same spacing. Such strategy works perfectly well for approximately symmetric volumes but should be adjusted for significantly asymmetric ones.

We call this algorithm *improved rotation estimation* later in the text. A comparison with basic version is shown in the experimental section of the paper.

3.3. Rigid body registration

Rigid body transform is a transform that combines rotations and translations. Finding optimal parameters of a rigid body transform (six parameters in 3D) is a very common task in image registration (Zitová and Flusser, 2003) (intra-subject studies, multimodal registration, etc). As it is mentioned in the introduction, there is a class of registration methods that employ a numerical optimization process to find the optimum of similarity measure on a space of parameters of a transformation model. Our algorithm uses above-described procedures to find parameters of rigid body transform so that the PCM metric – the correlation of whitened images – reaches its maximum. The optimization runs in iterations. Each iteration aims to improve the measure with respect to some subset of parameters. Such optimization resembles some well-known optimizers (e.g. Powell's direction set method Press et al., 1992) and is sometimes called *alternating optimization*. We call the algorithm described in this section cylindrical phase correlation method (CPCM).

Let us start with the identity transform T and a set of three linear independent axes. For example x , y and z are a suitable selection. We repeat the following iterations to compute a transform update T_{upd} :

Odd iterations compute PCM to estimate the shift between the reference volume f_R and moving volume transformed by actual transform $T(f_M)$.

$$T_{\text{upd}} \leftarrow \text{PCM}(f_R, T(f_M)).$$

Even iterations estimate the rotation component with respect to one of the axes by above-mentioned procedure.

$$T_{\text{upd}} \leftarrow \text{IRE}_{(x|y|z)}(f_R, T(f_M)).$$

Axes cyclically alternate as the algorithm advances so that for example in iterations 2, 4, 6, 8, 10, ..., axes x, y, z, x, y, \dots are used, respectively.

After each iteration, the current transform T is updated by new

$$T_{\text{upd}}$$

$$T \leftarrow T \circ T_{\text{upd}}.$$

This iterating process is terminated if there is no non-zero update found in the last six iterations (no transform parameter can be further optimized), or if the maximum number of iterations is met (time limit) or if the actual result is satisfactory (e.g. algorithm is stopped by an operator).

The convergence of our algorithm faces similar problems as common optimization techniques. It is not ensured that the attained optimum will be the global optimum of the similarity metric and that it is approached in some well-defined time limit. But in contrast to other methods our method is *optimal in every step* (PCM and IRE find the global optimum with respect to the given parameter subset). Furthermore, in the case of PCM, the optimum is found over three shift parameters in one step. Hence, the method should be capable of registering images with low spatial correlation and with high initial misregistration, which are usual properties that limit other methods. Again (as can be seen in experimental results) this does not guarantee the convergence to global optimum.

4. Experimental results

In this section, we present several experiments that study the method's performance. First, an influence of non-ideal conditions on PCM estimation of rotation angle on cylindrically mapped images is studied along with the performance of the improved algorithm in the same situation. In the second experiment, we discover the behaviour of CPCM on various initial misalignments and give certain conclusions about the accuracy, speed and robustness of the method. Consequently, we show the method's dependence on the selection of the axes set. In the fourth experiment, CPCM is compared with some reference methods. As all these experiments are simulated, we finally execute the method on a real data set in a real registration task.

In all experiments, we run our C++ implementation of the algorithms on an ordinary contemporary PC. The method is implemented as a module to Insight toolkit ITK (Ibanez et al., 2005).

4.1. Influence of noise and rotation axis error on rotation estimation

Algorithms for estimation of rotation angle (Sections 3.1 and 3.2) were tested for robustness under non-ideal conditions. First, we want to examine the influence of these conditions on an algorithm's behaviour and second, we want to justify the improvements given in Section 3.2.

In the first part of this experiment, a simulated MRI brain image (Fig. 1) was rotated around fixed axis by a random angle (from full 2π range) and Gaussian noise was added to the rotated image. The rotation angle was then recovered by both basic and improved versions of the algorithm and an absolute difference between the estimated and the original angle was measured as an estimation error. We generated many random angles for each level of noise with a new instance of noise for each measurement. Fig. 3a shows averaged errors over all measurements for each level of noise. Fig. 2 shows slice of MRI volume affected by -30 dB noise.

The second part of this experiment was similar but instead of adding noise we shifted the rotation axis in a random direction. Hence, the algorithms were estimated rotation around different axes than when the image was originally rotated (note that these

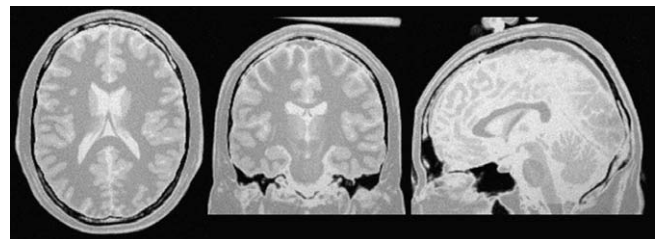


Fig. 1. BrainWeb (Collins et al., 1998) simulated MRI brain image. Volume size is $181 \times 217 \times 180$ with regular 1 mm spacing in all dimensions.

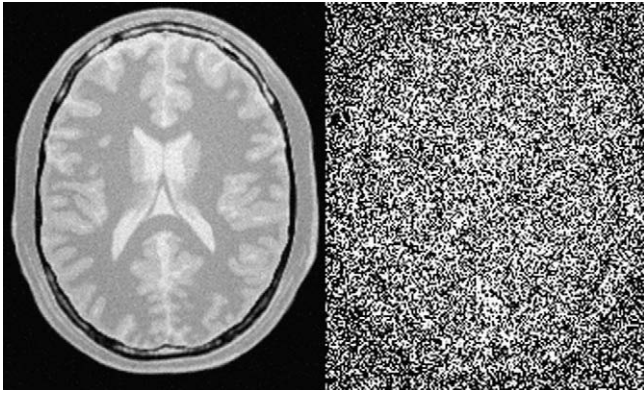


Fig. 2. BrainWeb image affected by noise of -30 dB. Such image pair is registered successfully by both basic and improved versions of the method. (In the image, noise is thresholded to fit in the range of $(0, 255)$.)

algorithms may not recover original rotation axis). Fig. 3b shows dependency of rotation angle error on the distance of the axis shift (again, the error was averaged over many measurements for each shift distance).

Algorithms proved extreme robustness with respect to noise. This can be explained due to the averaging nature of the PCM: we search for a single peak (ideally delta function) in a correlation surface which is a result of an inverse DFT of frequency spectra combined from the two images. The single peak is a kind-of-average (linear combination) of all frequency samples that are affected by the same noise as spatial samples of the original images. The variance of noise is reduced by averaging, hence, thanks to the large number of samples of 3D volume, the error of estimated rotation angle is low even for extreme noise.

If the rotation axis is shifted during rotation estimation, the algorithms were able to recover the angle as long as some structures in the data match. In both parts of the experiment, there is a clearly observable positive effect of the improvements given in Section 3.2. The effect of noise as well as the effect of disturbances is reduced between the two images (shifting the axis affects mainly the area near the rotation axis which causes most problems in the basic version of the algorithm). Hence, an improved algorithm is recommended and used in further experiments in this paper.

4.2. 3D rigid registration performance

Next, we aim to study the influence of initial misregistration level on the rigid body registration result and the number of itera-

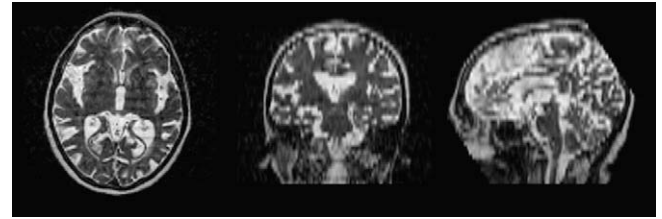


Fig. 4. Real MRI brain image. Volume size is $128 \times 128 \times 40$ with $1.8 \times 1.8 \times 4.58$ mm spacing.

tions needed to converge the algorithm. We use CPCM to register a randomly rotated and shifted real MRI brain image (Fig. 4) with the original. The degree of misregistration as well as the registration error is measured by a fixed set of eight points that uniformly sample the reference image's volume. The error (or misregistration) is then measured as a mean Euclidean distance of these points in moving image to their original counterparts in reference image. This could be understood as a mean distance of every point of a volume to its transformed counterpart.

We continuously generated random transforms, so that there was at least one hundred different transforms for each 1 mm level of initial misregistration. For each misregistration level, the results are the mean values over all transforms that introduced misregistration of that level. The graph in Fig. 5a shows two alternative views of the results. First, we filtered only those results that successfully converged under some reasonable error (here 10 mm – explained below). Then the graph also plots values that include all results. Fig. 5b shows the statistics of three kinds of failures:

1. The method converged (e.g. stopped automatically) but the final error was larger than the initial misregistration (the alignment was downgraded).
2. The method reached the iteration limit (120 iterations) before it was able to reduce the misregistration below 10 mm.
3. None of the two cases but the final misregistration error was still larger than 10 mm (the method got trapped in the local solution).

The results can be interpreted in the following fashion: until misregistration is about 100 mm, the method converges to the pixel-level precision with at least 90% reliability and the number of iterations (i.e. time) behaves approximately logarithmic to the misregistration. As misregistration grows over 100 mm (which is approximately the radius of the volume), the failure rate increases

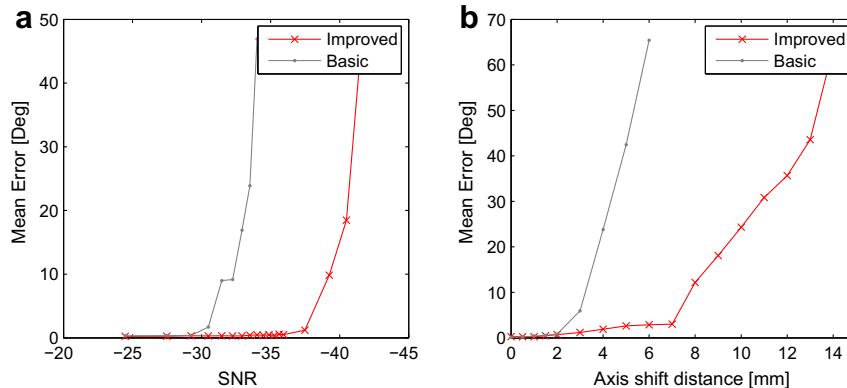


Fig. 3. Influence of noise and axis error on rotation estimation. The BrainWeb image is rotated by a random angle around a known fixed axis. (a) The rotated image is affected by a random Gaussian noise. (b) The rotation axis is shifted in random direction. In both cases, the image is registered by the presented rotation estimation algorithm (basic and improved versions). The graphs show the registration error (in degrees) averaged over many such registrations of random rotations, according to the level of introduced error.

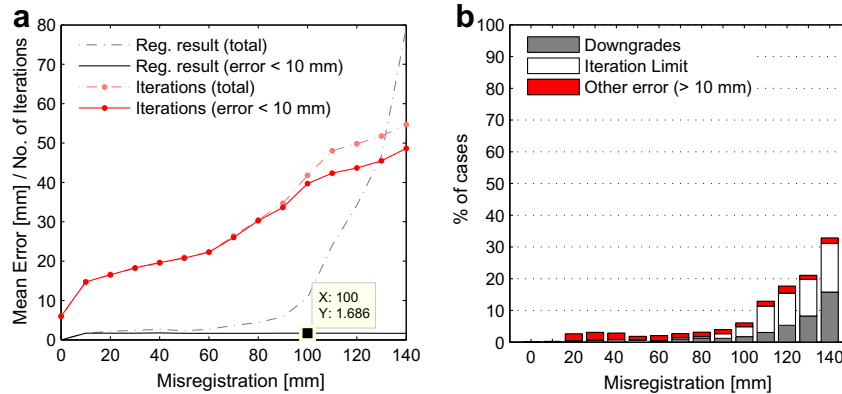


Fig. 5. Influence of initial misregistration on the mean error after registration (a), number of iterations (a) and failure statistics (b): cases of even increased initial misregistration (Downgrades), cases of reaching the iteration limit and the rest of the cases when the final misregistration was not decreased below 10 mm. For each bar, one thousand of random transforms were generated.

and the method's performance decreases mainly due to cases in which the method converged to some false position. We should point out that these results and trends do not depend on the specific value of *reasonable error* mentioned above. We use the value of 10 mm that is one order higher than the pixel size and is still reasonably small, but we could use values 5–45 mm without any significant effect on the graphs.

4.3. Axes selection influence

As stated in Section 3.3, we make no presumption about the data content and position so that the choice of the axis set is arbitrary. In this experiment we will show if the results of the method change with the selection of a different axes set.

First we took the real MRI brain image (Fig. 4), rotated it around the axis crossing points $[0,0,0]$ and $[1,1,1]$ by an angle α and shifted it in direction of x -axis by d millimetres. Then the original image and the transformed copy were rotated by a random rotation around a centre of the original image to reorient the pair with respect to x , y and z axes.

Table 1

Mean registration error with respect to various axes sets. One thousand random axes setups were generated for each configuration of original and transformed image.

α - d	Total mean error before/after registration
$10^\circ - 30$ mm	32.0 mm/2.0 mm
$25^\circ - 20$ mm	36.4 mm/5.0 mm

Table 2

Reference methods. The implementations are taken from ITK toolkit, the meanings of the parameters can be found in ITK Software Guide (Ibanez et al., 2005).

Abbreviation	Description	Parameters
General parameters	Dimensions of parametric space of rigid body transform corresponding to rotation parameters must be scaled relatively to translation parameters (step of 1 radian has different effects than step of 1 mm)	Rotation step = 1/200 rad Translation scale = 1 mm maximum Iterations = 600
POW	Powell's direction set optimization of correlation of whitened images. Represents similar type of optimization (alternating optimization) of the same metric	Step length = 0.02 Step tolerance = 0.001
MSE	Regular step gradient descent minimization of mean squared error. A well-known and widely used type of optimization of a metric usual for single-modality registration	Maximum step = 0.2 Minimum step = 0.01 Relaxation factor = 0.6
MI	Regular step gradient ascent maximization of Mattes mutual information. Usual state-of-the-art method for multi-modality registration	Maximum step = 0.2 Minimum step = 0.01 Relaxation factor = 0.5 # Of histogram bins = 50 # Of spatial samples = 10^5

Table 1 contains the results of the experiment. By changing the axes set the optimization procedure takes a different route through the parameter space and is therefore exposed to different local extremes. By choosing a different axes set the method may reach different results in the individual case and may even fail. But the overall performance over many cases complies with the results presented in other experiments.

4.4. Comparison to reference methods

The fourth experiment is intended to compare the new method with some classical as well as similar methods. We would like to compare the performance and robustness of the methods under various input conditions. Implementations of all reference methods are taken from Insight toolkit and any details on the methods and parameters can be found in Ibanez et al. (2005) and in public source codes of the toolkit.

Table 3

Success rate of the methods. All methods were executed on the same inputs. First column displays the misregistration level: X - Y denotes rotation by X degrees around random axis and shift by Y millimetres in random direction.

	CPCM (%)	POW (%)	MSE (%)	MI (%)
$5^\circ - 5$ mm	100.0	85.7	100.0	100.0
$15^\circ - 35$ mm	97.7	3.3	100.0	100.0
$60^\circ - 80$ mm	97.3	0.0	76.0	33.7
$120^\circ - 100$ mm	89.7	0.0	35.7	1.3
$5^\circ - 80$ mm	100.0	0.0	94.3	62.3
$60^\circ - 5$ mm	90.3	0.3	100.0	87.9

Table 2 lists reference methods along with the parameters. Tuning parameters of these methods to ensure fast, robust and accurate convergence is a very delicate task. A rather loose setting was selected to cover wider range of inputs and conditions. CPCM is not included in the table as it is described in the text and requires no parameters.

All methods are executed on the same inputs. MRI brain image (Fig. 4) is rotated by a fixed angle around random axis (crossing cen-

tre of the volume) and then shifted in a random direction by fixed distance. We selected a set of six combinations of fixed rotation angle and shift distance. The first four combinations represent increasing misregistration in both rotation and translation. The fifth combination is a large shift with a small rotation and the last is a small shift with a large rotation. Many (300) instances for each fixed combination are evaluated in the same way as in the previous experiment, each time with new random axis and shift direction.

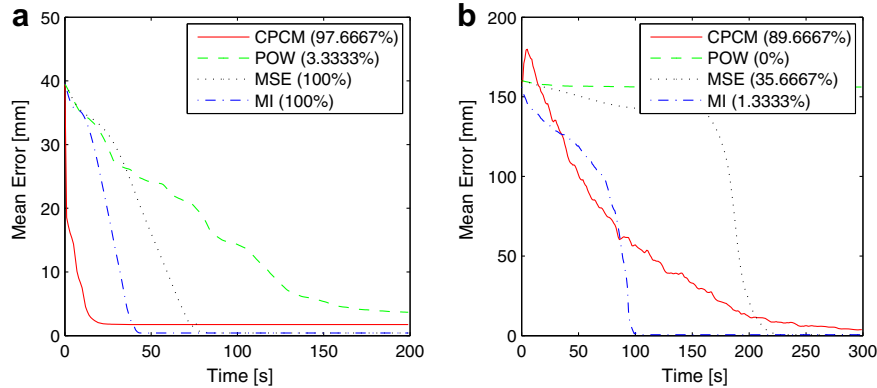


Fig. 6. Averaged successful runs. Graphs show how the misregistration is decreased in time by every method. Initial misregistration is 15°, 35 mm (a) and 120°, 100 mm (b). Values are averaged over 300 instances with random rotation axis and shift direction. Percentages in graph legends show the success rate. Note that CPCM reaches subpixel precision as expected.

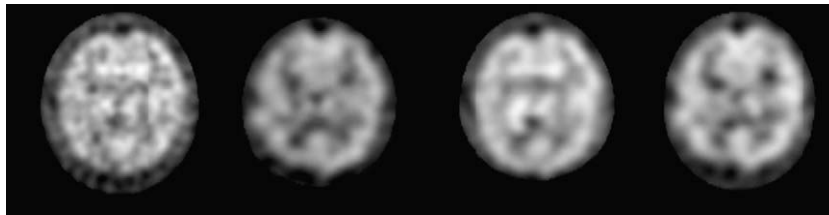


Fig. 7. SPECT brain image set (medial transversal slices). Volume size is 128 × 128 × 69 with regular 1.7 mm spacing in all dimensions.

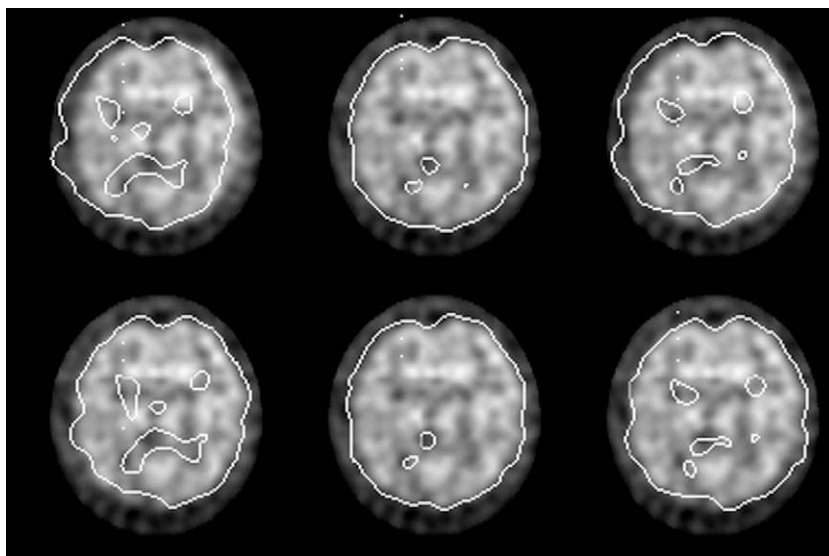


Fig. 8. Real registration result (medial transversal slice of first SPECT image overlaid by corresponding contour of the second, third or fourth image). First row shows initial position before registration and second row shows the registration result. The contours are generated as isocountours.

Table 4

Execution times in SPECT registration task. First column corresponds to registration of second image to first image, and so on.

	1–2	1–3	1–4
CPCM (s)	14.0	14.0	13.0
MI (s)	20.7	9.9	15.7

Table 3 shows success rates of all methods. The successful run of a method is defined in the same way as in the previous experiment: the misregistration is decreased below 10 mm. We can see that the success rate of all methods decreases with increasing misregistration but CPCM is affected at least. The low success rate of POW method is caused mainly by low spatial correlation of whitened images. The lower success rate of MI than that of MSE is caused by a limited number of samples from which the mutual information is computed. On the other hand, further results show that the implementation and setting of MI method ensures much faster convergence in successful runs than that of MSE.

Fig. 6 contains graphs of averaged successful runs of all methods on (a) small and (b) large initial misregistrations. CPCM rapidly decreases misregistration at the early phase of the optimization and then reaches result with lower speed and pixel-level resolution (note that the presented method is not supposed to work with sub-pixel precision). Gradient methods reduce most of the misregistration at the final phase of the optimization and reach subpixel accuracy, but with significantly smaller success rate. Selected implementation of MI runs faster than that of MSE but has smaller success rate. POW method was included just to illustrate a similar type of optimization and has a very low performance to be used in practice.

4.5. Real experiment

Finally, we employed CPCM in a real registration task. Fig. 7 shows a series of four SPECT brain images of a single patient which differ from each other by the acquisition time and state of the subject. The set consists of pre- and post-treatment images of a single patient who suffered a stroke, acquired in normal state and under pharmacological load. Our goal was to co-register all volumes. For the purposes of this experiment, we decided to register the last three volumes to the first one. We also compared the results and execution times with the MI method.

Fig. 8 shows the position of reference and moving volumes before and after registration. The result conforms to the previous experiments: after registration, volumes are still slightly misregistered, as CPCM is able to reach only pixel-level precision. MI method was able to reach higher (subpixel) precision but in mostly higher time (Table 4).

5. Conclusion

We presented a new image registration algorithm that is able to align geometrically mutually translated and rotated pairs of 3D images. The method iteratively recovers the translational component of misalignment by PCM and rotational component of misalignment by applying PCM on cylindrically mapped images.

The method's performance was examined in several experiments and compared to several reference methods. CPCM shows very low sensitivity to noise and is able to rapidly reduce even a large initial misalignment, which is a common limitation, for example, for methods based on Mutual information. On the other

hand, the current method is able to register images only with pixel-level precision. Employment of CPCM in various applications is eased by absence of any parameters which often decrease applicability and universality of other methods. CPCM can also be easily parallelized for multi-core and multi-processor machines and accelerated by hardware implementation of FFT.

We also considered a direct extension of the method for the subpixel precision by applying one of the subpixel solutions published by other authors. There are several problems and complications with such solution so we decided to keep this presentation of the main method and the principle as clear as possible and we left the detailed study of the subpixel possibilities for the future. The main complications are the stability of most of the methods (low stability leads to bad termination criteria) or their computational complexity, also the subpixel resolution is not required in all applications. A good and powerful solution would be to use CPCM in combination with some gradient method to fine-tune the result of CPCM to subpixel precision or to use one of the subpixel modifications of phase correlation for the last iteration. Another improvement might be an intelligent selection of the axes set at the beginning or even during the optimization, for example by detecting the main rotation axis from the data and/or the actual intermediate transform.

These properties nominate CPCM mainly for single-modality, intra-subject 3D registration tasks. It can also be used in approaches that approximate the non-rigid motion by piece-wise rigid motions (e.g. Walimbe and Shekhar, 2006). Although the experiments were run only on a small set of data, the method's behaviour was very stable, which is promising for its usage for large variety of data even outside medical image analysis area.

Acknowledgements

The authors would like to thank the Czech Ministry of Education for support under the Project No. 1M0572 (Research Center DAR), the Charles University in Prague for support under the project GAUK 48908 (Medical Image Registration and Fusion) and the Czech Science Foundation (GA CR) for support under the Project No. 102/08/1593.

References

- Baker, M., 1998–2007. <www.euclideanspace.com>: Maths – rotations. URL <http://www.euclideanspace.com/maths/geometry/rotations/index.htm>.
- Collins, D.L., Zijdenbos, A.P., Kollokian, V., Sled, J.G., Kabani, N.J., Holmes, C.J., Evans, A.C., 1998. Design and construction of a realistic digital brain phantom. *IEEE Trans. Med. Imaging* 17 (3), 463–468.
- De Castro, E., Morandi, C., 1987. Registration of translated and rotated images using finite Fourier transform. *IEEE Trans. Pattern Anal. Machine Intell.* 9 (5), 700–703.
- Foroosh, H., Zerubia, J., Berthod, M., 2002. Extension of phase correlation to subpixel registration. *IEEE Trans. Image Process.* 11 (3), 188–200.
- Gholipour, A., Kehtarnavaz, N., Briggs, R., Devous, M., Gopinath, K., 2007. Brain functional localization: A survey of image registration techniques. *IEEE Trans. Med. Imaging* 26 (4), 427–451.
- Hoge, W., 2003. A subspace identification extension to the phase correlation method. *IEEE Trans. Med. Imaging* 22 (2), 277–280.
- Hoge, W., Westin, C., 2005. Identification of translational displacements between n -dimensional data sets using the high-order svd and phase correlation. *IEEE Trans. Image Process.* 14 (7), 884–889.
- Ibanez, L., Schroeder, W., Ng, L., Cates, J., 2005. *The ITK Software Guide*, second ed. Kitware, Inc. ISBN 1-930934-15-7. <http://www.itk.org/ItkSoftwareGuide.pdf>, URL <http://www.itk.org/ItkSoftwareGuide.pdf>.
- Keller, Y., Averbuch, A., Miller, O., 2004. Robust phase correlation. In: *Internat. Conf. on Pattern Recognition*, II, pp. 740–743.
- Keller, Y., Shkolnisky, Y., Averbuch, A., 2006. Volume registration using the 3D pseudopolar Fourier transform. *IEEE Trans. Image Process.* 15 (11), 4323–4331.
- Kuglin, C., Hines, D., 1975. The phase correlation image alignment method. In: *Proc. Internat. Conf. on Cybernetics and Society*, IEEE, pp. 163–165.

- Press, W., Flannery, B., Teukolsky, S., Vetterling, W., 1992. Numerical Recipes in C, second ed. Cambridge University Press.
- Reddy, B., Chatterji, B., 1996. An fft-based technique for translation, rotation, and scale-invariant image registration 5 (8), 1266–1271.
- Stone, H., Orchard, M., Chang, E., Martucci, S., 2001. A fast direct Fourier-based algorithm for subpixel registration of images. IEEE Trans. Geosci. Remote Sensing 39 (10), 2235–2243.
- Walimbe, V., Shekhar, R., 2006. Automatic elastic image registration by interpolation of 3D rotations and translations from discrete rigid-body transformations. Med. Image Anal. 10 (6), 899–914.
- Zitová, B., Flusser, J., 2003. Image registration methods: A survey. Image Vision Comput. 21 (11), 977–1000 <[http://dx.doi.org/10.1016/S0262-8856\(03\)00137-9](http://dx.doi.org/10.1016/S0262-8856(03)00137-9)>.